Label-free Surface Plasmon Resonance Biosensing with Titanium Nitride Thin film

Guangyu Qiu, Siu Pang Ng, Chi-Man Lawrence Wu

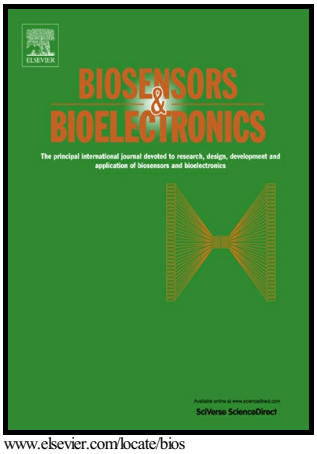

www.elsevier.com/locate/bios

PII: S0956-5663(18)30093-9
DOI: https://doi.org/10.1016/j.bios.2018.02.006
Reference: BIOS10268

To appear in: *Biosensors and Bioelectronic*

Received date: 25 November 2017
Revised date: 5 January 2018
Accepted date: 1 February 2018

Cite this article as: Guangyu Qiu, Siu Pang Ng and Chi-Man Lawrence Wu, Label-free Surface Plasmon Resonance Biosensing with Titanium Nitride Thin film, *Biosensors and Bioelectronic,* https://doi.org/10.1016/j.bios.2018.02.006

Label-free Surface Plasmon Resonance Biosensing with Titanium Nitride Thin film

Guangyu Qiu, Siu Pang Ng*, Chi-Man Lawrence Wu**

Department of Materials Science and Engineering, City University of Hong Kong, Hong Kong SAR, P. R. China

Siu Pang Ng (corresponding author): rollyng@cityu.edu.hk*

*Chi-Man Lawrence Wu** (corresponding author): lawrence.wu@cityu.edu.hk*

Abstract:
In this report, titanium nitride thin film synthesized with reactive magneto-sputtering technique is proposed as an alternative surface plasmon resonance sensing material. The physical and chemical natures were initially studied by atomic force microscopy, X-ray diffraction and X-ray photoelectron spectroscopy. In virtue of white-light common-path sensing system, the wavelength modulated TiN films achieved tunable evanescent plasmonic field from 573nm to 627nm. The optimized TiN film with 29.8nm thickness exhibited good differential phase sensitivity (i.e. 1.932×10^{-7} RIU) to refractive index alteration, which is comparable to the performance of gold film. We have also attained direct measurement of biotin adsorption on the TiN and monitored sub-sequential biotin-streptavidin conjugation. It was found that TiN films have significantly higher binding affinity toward biotin than that of gold in experiments, so we are able to detect biotin directly to 0.22 μg/ml (0.90 μM) in label-free manner. The adsorption mechanism of biotin on TiN(200) are also explored with periodic density functional theory (DFT) via computer simulation and it was found that the exceptional biotin-TiN affinity may be due to the stacking formation of both N-Ti and O-Ti bonds. Also, the adsorption energy of biotin-TiN was found to be -1.85 eV, which was two times higher than that of biotin-gold. Both experimental and computational results indicate, for the first time, that the TiN film can be directly functionalized with biotin molecules, thus it serves as an alternative plasmonic material to existing gold-based SPR biosensors.

Keywords: Surface plasmon resonance; Titanium nitride; Biosensor; Biotin; Density functional theory;

1. Introduction

Surface plasmon resonance (SPR) is the light induced coherent electrons oscillation and electromagnetic waves propagation at the planar interface of dielectric-conducting media. Abundant scientific studies utilized surface plasmons (SPs) effect to convert photon energy into electron oscillation and make SPR attractive for use in many actual or potentially useful applications such as electronic devices (Schuller et al. 2010), biosensing (Homola et al. 1999), catalysis (Tian and Tatsuma 2005) and photochemistry (Uechi and Yamada 2008). Since the first attempt in biosensing application (Liedberg et al. 1983), the great potential of SPR sensing method has been receiving growing interest in scientific and commercial community. SPR based biosensors have been proven to have excellent capability in studying biomolecular interaction, chemical detection, medical diagnostics and immunoassays (Shankaran et al. 2007; Vo-Dinh and Cullum 2000). Most of these works used gold (Au) as the plasmonic materials. Au is the primary plasmonic media as the element supports plasmon resonance in the middle of the visible range, and exhibit good resistance to oxidation, non-toxic and readily fabricated into nanostructures. A few other elements are also possible candidates for application in plasmon resonance. Silver (Ag) exhibits excellent plasmon resonance performance at the blue end of the visible region (Weimer and Dyer 2001), but is susceptible to oxidation over short timescale. Furthermore, alkali metal elements such as lithium,

potassium and sodium also have strong plasmon resonance in the visible range, but would oxidize rapidly without inert gas protection (Mann and Broida 1973).

Transparent conducting oxides (TCOs) have been considered as better plasmonic materials that have better processibility and durability (Michelotti et al. 2009) than conventional ones. However, the TCOs fail to exhibit plasmonic resonance in the visible region, as the carrier concentration is limited at around 10^{21} cm^{-3}. The optical properties of tin-doped indium oxide (ITO), which is one of intensively studied TCOs, have been investigated widely and its plasmonic resonance can be varied from 1600 nm to 2200 nm by controlling the concentration of Tin doping (Kanehara et al. 2009). On the other hand, transition metal-nitrides (TMNs) exhibit higher carrier concentration than that of TCOs, making them suitable to provide plasmon resonance in the visible or near-infrared region (Comin and Manna 2014). Titanium nitride (TiN), a ceramic TMNs material with exceptional physical and chemical properties, has attracted tremendous scientific and technological interest in past decades. Its attributes, including high hardness, low resistivity, corrosion resistance and tunable optical absorption make them very attractive for applications such as abrasion resistant coating, corrosion resistant coating, surface decoration coating and diffusion barrier layers (Chen et al. 2003; PalDey and Deevi 2003). Generally, TiN shows good plasmonic response in near infrared region as the smaller carrier concentration than that of noble metals, such as gold and silver. The recent studies have indicated that the optical properties of TiN may be tuned by changing the processing conditions (Naik et al. 2012) and structure dimensions (Venugopal et al. 2017). Several studies have proposed TiN as an alternative plasmonic materials for gold, for example, in the application of surface enhanced Raman Spectroscopy (SERS) (Zhao et al. 2015), solar heat transducers (Ishii et al. 2016), solar water splitting (Naldoni et al. 2017) and plasmonic absorber for photovoltaic devices (Wang et al. 2015). Computational and experimental works (Wang et al. 2015) has proved that TiN thin film and nanostructure exhibits potential to absorb broadband photon energy with high convert efficiency based on the plasmonic properties. Although the promised optical plasmonic properties of TiN have been studied (Cortie et al. 2010; Patsalas et al. 2015), and most of them predicted the possibility of TiN based SPR sensors, there are only a few studies that utilized TiN in the SPR application of biological or chemical sensing (Dong et al. 2011; Zhao et al. 2015), in which a narrow and sharp absorption should be necessary (Mayer and Hafner 2011). Currently, most of the biological sensors, chemical sensors and ambient environment sensors (pH value) of TiN materials are based on potentiometric methods, synthesized field effect transistor and electrochemistry approaches (Chin et al. 2001; Dong et al. 2011; Haldorai et al. 2016; He et al. 2015; Kong et al. 2016; Liu et al. 2016).

In the present work, we report direct growth of TiN thin film on BK7 glass substrate by reactive magnetron sputtering methods. It will be shown that TiN thin film has tunable plasmonic absorption in middle visible region. Based on the common-path optical sensing system (Ng et al. 2013; Qiu et al. 2015), TiN film exhibited good SPR sensing performance toward ambient refractive index under both wavelength modulation and phase modulation methods. Under the excitation of white light, the TiN film also shows a wide dynamic sensing range. In addition, our experimental and computational studies indicated that TiN film has good adsorption toward biotin molecules compared to that of gold film, which indicated its potential for further biosensing applications.

2. Material and Methods

2.1 Deposition of TiN film

TiN film can be synthesized by a variety of methods, such as direct current reactive magnetron sputtering (Elstner et al. 1994), pulsed laser deposition (Major et al. 2004) and thermal nitridation of Titanium dioxide at elevated temperature (Li et al. 2001). In this work, the ultrathin TiN films were fabricated with radio-frequency (RF) magneto-sputtering (Edwards Coating system E306A) from a titanium metallic target (99.999% pure). In detail, the cleaned glass substrates were initially mounted on the rotating fixture

and evacuated to a base pressure of 10^{-7} Torr. During the magnetron sputtering with 100W RF power, the vacuum was at 6×10^{-3} Torr and the Ar and N_2 flow was kept at 17.5 sccm and 7 sccm, respectively. The film thickness was controlled by monitoring the sputtering time duration. In order to compare the biosensing performance with conventional Au, 50 nm Au film was synthesized by magnetron sputtering system with 60W DC power and the thickness is controlled by quartz crystal monitor. The appearances of synthetic TiN film and Au film are shown in Fig. S1.

2.2 Plasmonic sensing system

In order to investigate the SPR sensing performance of TiN film, the common-path white light SPR system was used to perform the detection of ambient refractive index (RI) as well as biotin molecules adsorption (Ng et al. 2013; Ng et al. 2011; Qiu et al. 2015). In this work, the sensing performance of TiN films with various thickness were all primarily examined with a wavelength modulated SPR system, as shown in Fig. S2a. Then, more chemical and biology sensing investigations were conducted with phase modulation methods as shown in Fig. S2b. The operating procedure is also given in the supplementary material.

2.3 Sensing protocols

The sensing performance of TiN films toward ambient RI variation was initially examined with sodium chloride (NaCl) solution and the RI value can be linearly controlled from 1.333 RIU to 1.368 RIU by changing the NaCl concentration from pure deionized water to 20 wt% (Weast 1988). Generally, the NaCl solution was directly injected into the probe cell with Peristaltic pump at a constant rate of 0.2 ml/min. The wavelength or phase response was recorded by the spectrometer (Avantes, Avaspec-ULS2048TEC) with the associated software AvaSoft-Avantes in real time.

Biotin (Sigma-Aldrich, USA) and streptavidin (Sigma-Aldrich, USA) are all in analytical grades and directly diluted with an appropriate amount of 0.01 M phosphate buffered saline (PBS, Sigma-Aldrich, pH 7.4 at 25 °C, containing 0.138 M NaCl; 0.0027 M KCl) before the sensing experiments. The PBS solution was also employed as the running buffer in our experiments and pH 7.4 was the general environment for whole functionalization and detection process. In biotin molecular adsorption sensing studies, the PBS solution was initially injected into the probe cell by a peristaltic pump at constant rate of 50 µL/min to build the baseline. Then the biotin in PBS was injected continuously for 20 minutes to ensure sufficient adsorption of biotin molecules on TiN film surface. The TiN film was subsequently rinsed by PBS buffer to check the binding affinity between TiN and biotin molecules. Further confirmation of the biotin adsorption was carried out by injecting streptavidin solution into the probe cell and recording the phase response successively.

2.4 Computational investigation of biotin adsorption on TiN(200)

In order to study the adsorption mechanism of biotin molecule on the TiN film, the adsorption energy via each functional group of the biotin molecule attaching to the TiN(200) surface was calculated via density functional theoretical (DFT) at the ground state using the open-source Quantum Espresso package (Giannozzi et al. 2009). Generalized gradient approximation (GGA) with Perdew-Burke-Ernzerhof (PBE) functional (Perdew et al. 1996) was selected to describe the exchange-correlation interaction. Van der Waals (vdW) interactions were considered using the Grimme's DFT-D2 method (Grimme 2006). The kinetic energy cutoff for wavefunctions and density were 55 Ry and 440 Ry as given by standard solid state pseudopotentials (Lejaeghere et al. 2016). The convergence threshold of 10^{-4} Ry/Borr for total energy and 10^{-3} Ry for total force were used. In order to construct the TiN(200) surface, the primitive cell of TiN was fully variable-cell relaxed. Then, the TiN(200) surface was constructed by cubic 4 × 6 × 3 TiN supercell (12 Å × 18 Å × 4 Å) with a sufficiently vacuum slab of 25 Å built along the *z* axis to avoid interaction of duplicated images. For sampling the Brillouin zone, Monkhorst-Pack k-point (Monkhorst 1976) was set as 4 × 4 × 1, and a larger 8 × 8 × 1 k-point was used to investigate the electronic properties.

The biotin molecule was placed initially in the middle and on the top of the TiN slab with touching contact via different functional groups. The initial configurations of each orientation are shown in Fig. S3 and the corresponding positions after full relaxation are shown in Fig. 1. Fig. 1a is the biotin molecule with the carbonyl group (C=O) attaching to the TiN(200) surface; Fig. 1b is the biotin which anchors via the carboxyl group (COOH); Fig. 1c is with biotin lying flat to the surface; Fig. 1d is connected with the amine group (NH); and lastly Fig. 1e is positioned with the sulfide group (R-S-R'). There are a total of 176 atoms and 1314 valence electrons in these models, since both biotin and TiN(200) are non-magnetic, spin polarization was not considered in computing of the adsorption energy.

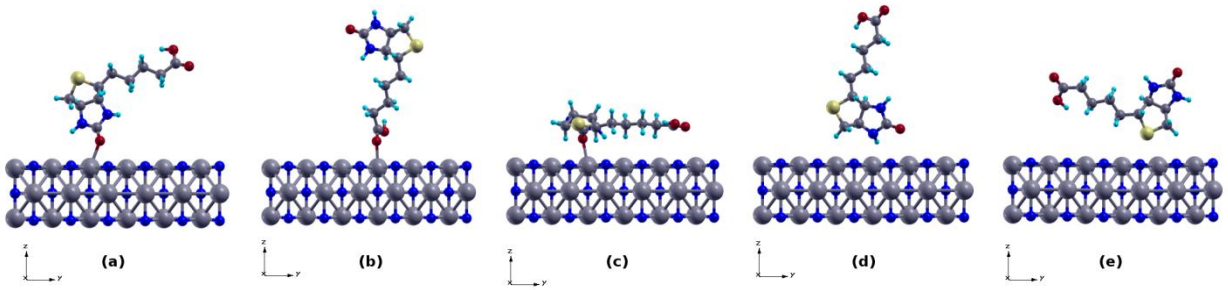

Fig.1. Fully relaxed geometry of biotin adsorption on the TiN(200) slab surface via (a) carbonyl, (b) carboxyl, (c) flat, (d) amine and (e) sulfide groups. The relatively larger dark gray spheres represent titanium, the dark blue spheres are nitrogen, the red spheres are oxygen, the yellow sphere is sulfur, the relatively small dark gray spheres are carbon of biotin, and the smallest light blue spheres are hydrogen.

The adsorption energy E_{adp} is defined as

$$E_{adp} = E_{TiN(200)+Biotin(fg)} - E_{TiN(200)} - E_{Biotin(fg)} \quad (1)$$

where $E_{TiN(200)+Biotin(fg)}$, $E_{TiN(200)}$ and $E_{biotin(fg)}$ are the total energies after relaxation. $E_{TiN(200)+Biotin(fg)}$ is total energy of the TiN(200) surface and the biotin molecule with one of its functional group oriented towards the surface. $E_{TiN(200)}$ is the total energy of the surface and $E_{Biotin(fg)}$ is the total energy of the molecule without the presents of the surface. It is believed the more the negative the E_{adp}, the lower the energy of the system at ground state, which may indicate the preferred adsorption geometry of the biotin molecule on TiN(200) surface, such that it may affect further functionalization of biomolecules i.e. biotin-streptavidin conjugation. The calculated adsorption energy, projected density of states (PDOS) and differential charge transfer for biotin adsorption on TiN(200) via each functional group is discussed in section 3.4.

3. Results and Discussion

3.1 Characterization of TiN thin films

The initial chemical confirmation of the synthesized TiN films and their crystal structure were investigated by X-ray diffraction (XRD, Rigaku SmartLab) with Cu-Kα radiation at 45kV. The diffraction peaks from synthetic TiN films on BK7 glass slide exhibited typical pattern of cubic TiN as shown in Fig. 2a. The TiN films are all polycrystalline with (200) preferred orientation. The texture coefficient of (111), (200) and (220) planes of the films are calculated by the following equation:

$$\text{Texture coefficient} = I(hkl)/[I(111) + I(200) + I(220)] \quad (2)$$

where I(hkl) represents the reflected intensity from (hkl) plane in XRD data. The calculated texture coefficents of (111), (200) and (220) of three TiN film are 0.27, 0.51 and 0.22 respectively. As the synthesis conditions were the same, all these films exhibited a strong (200) orientation and a relatively weak (111) and (220) orientations. The XRD suggested dominant (200) texture was utilized in the following adsorption simulation. Besides, a previous study has proved that the mechanical properties such as hardness and elastic modulus of TiN films changed with the crystal orientation (Patsalas et al. 2000). Also, the (200) crystal orientation can contribute to the enhancement of mechanical performance of TiN films.

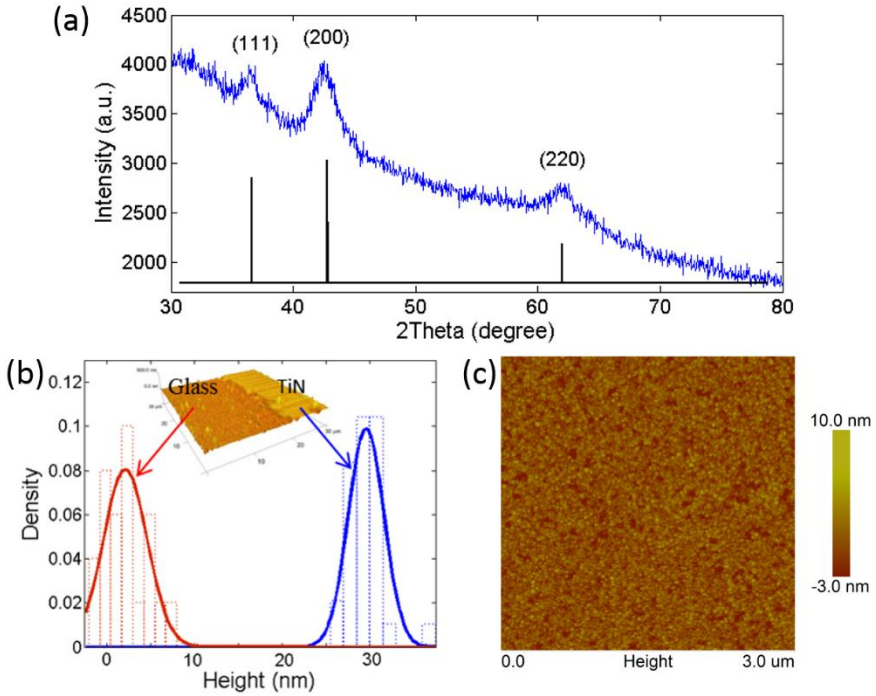

Fig. 2. (a) X-ray diffraction pattern of a film of TiN on BK7 glass substrate. The scanning range is 2θ from 30 degree to 80 degree. (b) Statistical analysis of TiN film thickness. The surface roughness of TiN film (in blue) and glass substrate (in red) were statistically plotted. (c) TiN film morphology and surface roughness investigated by AFM in 3×3 μm, with scale bar ranged from -3 to 10nm.

Three different TiN films thicknesses were used to investigate their SPR sensing performance. Also, tapping-mode atomic force microscopy (AFM) was used to confirm the thickness. By scanning the boundary of TiN films on BK7 substrate, the thicknesses were statistically calculated as shown in Fig. 2b. The surface roughness of TiN film (in blue) and glass substrate (in red) were statistically plotted and the mean thickness of TiN-2 film was found to be approximately 29.8 nm, as shown in Fig. 2b. The mean thickness of the other two samples, i.e. TiN-1 and TiN-3, were found to be 25.6nm and 34.1nm, respectively. Fig. 2c shows the surface RMS (root-mean-square) roughness of TiN films. The RMS roughness of synthetic TiN films was approximately 1.49 nm, thus indicated the dense structure of TiN film. It is noted that the RMS roughness of the glass substrate was similar at 1.18 nm. Furthermore, the grain size was investigated with AFM in a 500nm×500nm region. The topographic height, amplitude and phase images shown in Fig. S4 exhibit uniform nano-grain distribution with mean size of 24 nm. The AFM topographical study showed that the synthesized TiN films have good surface density and smooth surface roughness, indicating that the synthetic TiN films would have good mechanical properties (Chun 2013). Further chemical state study of synthesized TiN film were performed by X-ray photoelectron spectroscopy (XPS, Physical Electronics PHI5802 system), and the chemical details were discussed in the supporting material.

3.2 SPR sensing performance toward ambient RI

Several experimental and computational studies (Cortie et al. 2010; Guler et al. 2015; Naik et al. 2012) have suggested that TiN films could exhibit plasmonic effect in visible range, yet to the best of our knowledge, direct SPR sensing performed with TiN films is still absent. Here we utilized the common-path sensing system to investigate the plasmonic resonance of TiN and its optical response toward the variation of bulk RI variation. The reflected white light from the interface of TiN-film/dielectric media was recorded by the spectrometer, in which the output spectra contain the evanescent point as shown in Fig. 3a. Under white light illumination, the plasmonic absorption of TiN films with different thickness was compared directly. By changing the thickness of TiN films (i.e. from 25.6nm, 29.8 nm to 34.1 nm) and keeping the excitation condition unchanged, the resonance wavelength shifted from 573 nm to 585 nm and further reached 627 nm, as shown in Fig. 3a. Also, the TiN-2 film exhibited the strongest and sharpest absorption at approximately 585nm. Such resonance wavelengths can be further extended by changing the TiN structure, dimension and chemical compositions. Subsequently, the sensing performance of these three thickness cases was investigated initially by changing the bulk RI values. Here, four different solutions (deionized (DI) water, 4% NaCl, 8% NaCl and ethanol) were utilized to change the RI value from 1.333 RIU to 1.3614 RIU. The analyte solutions were injected into the probe cell with syringe pump continuously while the spectrometer recorded the reflected spectra. The shifts of the resonance wavelengths of sample TiN-2 were illustrated in Figs. 3b and 3c. Generally, the dip position of TiN-2 shifted to the long-wavelength linearly with increased RI value, and the responses of the three samples are compared in Fig. 3d. These data imply that the average bulk RI sensitivities (S) of the three TiN films are S_{TiN-1}=138.79nm RIU^{-1}, S_{TiN-2}=264.08nm RIU^{-1} and S_{TiN-3}=206.4nm RIU^{-1}, respectively. That is, TiN-2 exhibited the highest sensitivity and strongest plasmonic resonance in wavelength modulation. Based on the thin film characterization, the TiN film with 29.8 nm thickness exhibited the best sensing performance in current sensing system. Thus, the TiN-2 sample with 29.8 nm thickness was used to perform the SPR phase modulation to investigate the limit of detection and its dynamic range.

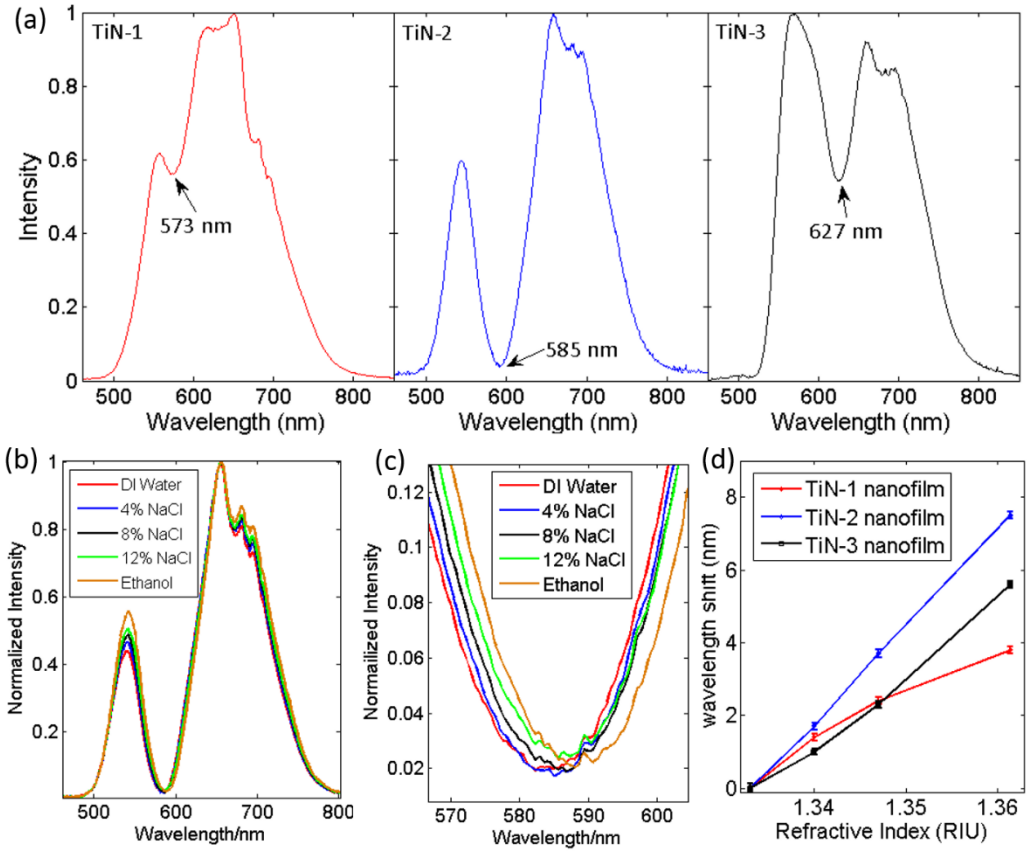

Fig. 3. SPR reflectance spectrum from (a) TiN-1, TiN-2 and TiN-3 films, with absorption dips presented at 573 nm, 585 nm and 627 nm respectively. (b) The TiN-2 film was subsequently tested with wavelength modulation methods with various RI solutions, and (c) the enlarged dips shifted proportional to the RI values. (d) The plot of wavelength shifts versus refractive index changes obtained from TiN films.

In the differential phase SPR sensing investigation, the interferogram oscillation significantly decreased at optimal resonance wavelength (590nm) as shown in Fig. 4a. The sensitivity of TiN-2 film is estimated by replacing the 2% NaCl solution with 4% NaCl solution, i.e. changing the refractive index from 1.3365 to 1.3400 RIU, and the interferogram response at 587nm was found to occur over a narrow response range. In order to calculate the differential phase, windowed Fourier transform (WFT) methods (Hlubina et al. 2008) was adopted to extract phase response from the interferograms, and the calculated phase has shifted by 3.17 radian, as shown in Fig. 4b. Considering the systemic blank measurement noisy and adopt the sensitivity calculation (Ng et al. 2011), the limit of detection (LOD) of phase modulated TiN-2 film is found to be 1.932×10^{-7} RIU. Compare to the literature of gold films SPR sensor, the phase modulated LOD were reported to be 2.6×10^{-7} RIU (Ng et al. 2011) and 2×10^{-8} RIU (Ng et al. 2013). It indicated our proposed TiN film has competitive sensitivity compared with conventional noble gold film. To investigate the feature of dynamic range, various NaCl solution concentrations, i.e. 2%, 4%, 6%, 8%, 10%, 12%, 14%, 16%, 18% and 20% by weight were successively injected into the probe cell every 600 seconds. The continuous sensing process was recorded in real time as shown in Fig. 4c. In contrast to the wavelength modulation, differential phase response was confined into a narrow region, which may contribute to the higher sensitivity. Here we selected single wavelength at 598 nm to investigate the systematic dynamic range, as shown in Fig. 4d. The initial based line was created by injecting 2% NaCl solution for 900 seconds. Then other NaCl solutions with various RI was injected to change the ambient dielectric media on TiN film. The differential phase response is proportional to the RI value from 1.3365

to 1.3684 RIU, i.e. RI range of 3.2×10^{-2} RIU. It is noted that the phase response from 18% NaCl to 20% is relatively lower than that of low concentration conditions, which indicated the plasmonic sensing position has gradually shifted to longer wavelength of 600nm, as shown in Fig. 4c. At the end of dynamic refractive index experiment, the initial 2% NaCl solution was injected again to check the reusability of TiN film. The final phase response value returned to the original baseline indicating the good reversibility of our proposed TiN film SPR sensors. The ambient-RI experiments with TiN film indicated the competitive sensitivity with conventional Au SPR, and similar dynamic range.

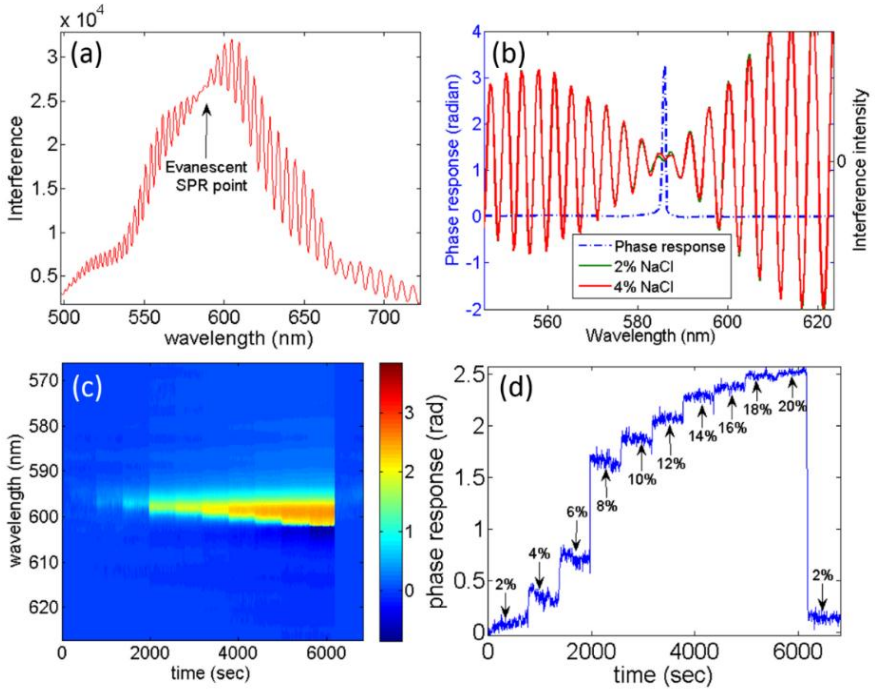

Fig. 4. (a) interferogram of TiN film with evanescent SPR point at 590 nm. (b) the evanescent point significantly changed toward two analytes, i.e 2% and 4% NaCl, and the calculated phase response as shown in blue curve indicated the sharp response of 3.17 radian. (c) and (d) illustrated the real time monitoring of successively injected NaCl solution from 2% to 20%.

3.3 Biotin adsorption on TiN thin films for potential biosensing applications

The initial SPR sensing characterization with inorganic analytes indicated that TiN films can be a strong candidate for bulk RI sensing. Here we utilized biotin (244.3 g/mol), a water-soluble B-vitamin biomolecule to test the direct adsorption onto TiN film. Biotin is a heterocyclic, S-containing monocarboxylic acid, and commonly served as the start point for the attachment of DNA (Fredriksson et al. 2002), antibody (Backmann et al. 2005) or other specific receptors (Balamurugan et al. 2008) for immune-sensing applications. In the experiment, the PBS solution was initially injected into the probe cell to build the baseline. Subsequently, the biotin diluted in PBS with various concentration, i.e. 100 ng/ml, 500 ng/ml, 1 μg/ml, 5 μg/ml and 10 μg/ml were detected by TiN films individually. For comparison, the gold film (with thickness about 50 nm) was also used to perform the biotin adsorption with 10 μg/ml biotin solution. As shown in Fig. 5a, the phase response increased steadily in the first 1200 second as various biotin solutions were injected. Afterwards, the PBS buffer solution was used to rinse the TiN films again to check the binding affinity between biotin and TiN, and resulting in slightly decreased phase response and stabilized in the case of 10 μg/ml biotin solution at 1200 seconds, which may indicated the saturation of biotin-TiN binding on the film surface. In the comparison test with Au film, biotin did not produce comparable phase response as shown in Fig. S6. For TiN-film sensors, the

final phase values towards different biotin concentration were provided in Fig. 5b to evaluate their linear sensing response and the LOD. The phase responses with standard errors were applied to linear fitting, which suggested that the linear relationship is $y=0.026\times x+0.00975$, where x indicated the biotin concentration in unit of μg/ml and y indicated the system phase response. As suggested by IUPAC (International Union of Pure and Applied Chemistry), the LOD of sensing system should be the sum of the mean of blank measurement (0.005 radian) and triple of its standard deviation (i.e. 3.5×10^{-3} radian). Thus, the LOD of TiN film is about 0.22 μg/ml (900 nM). Compared to LSPR biosensor with Au nanorod (Kabashin et al. 2009), TiN film shows competitive sensitivity to biotin by direct adsorption. These results suggested that the biotin can be utilized as the functionalization anchor for TiN surface modification. In order to further confirm the immobilization of biotin and check the bioactivity of adsorbed biotin molecules, we utilized the biotin-TiN films to detect streptavidin. The TiN films were initially functionalized with biotin molecules by two different concentrations, i.e. 1 μg/ml and 5 μg/ml. Then, streptavidin in PBS was injected into the probe cell. A significant increase in phase was observed when the streptavidin were added into the sensing chamber and combined with immobilized biotin molecules, as shown in Fig. 5c. The successive phase response from biotin adsorption and biotin-streptavidin interaction not only confirmed the strong binding affinity between biotin and TiN, but also indicated the immobilized biotin molecules have good bioactivity to conjugation of streptavidin. Moreover, the biotin functionalized TiN film maintained the plasmonic response in the visible sensing range and produced reliable phase response. These results confirm that TiN can be directly functionalized with biotin molecules and the TiN-biotin structure shows good SPR sensing performance. By combination with biotinylation technology and functionalized with biotinylated proteins, the TiN film should be applicable for biosensing of DNA and proteins.

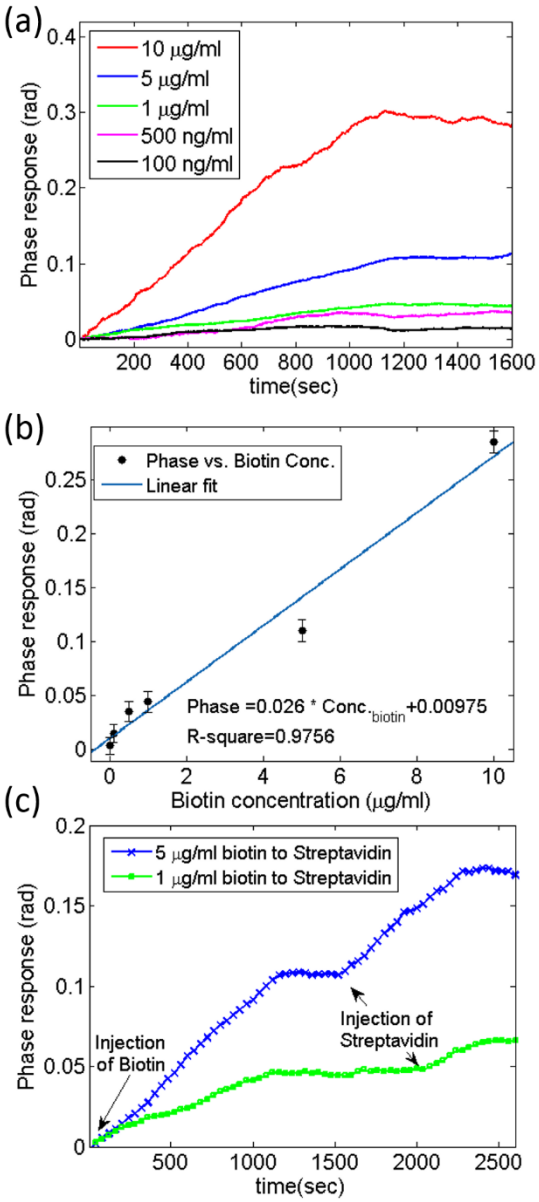

Fig. 5. (a) Phase modulated real-time response of TiN film toward various biotin concentrations in PBS. (b) The final phase responses versus biotin concentration were plotted and linearly fitted. (c) Successive detection of biotin and streptavidin with TiN films.

3.4 Computational investigation of biotin adsorption

The results of the DFT computation are summarized in Table 1 below.

Functional groups	Carbonyl (C=O)	Carboxyl (COOH)	Flat	Amine (NH)	Sulfide (R-S-R')
Adsorption energy (eV)	-0.63	-0.65	-1.87	-0.89	-0.12
Intermolecular distance (Å)	2.29	2.20	2.27	2.68	2.86
Maximum charge transfer (e)	0.99	1.04	1.00	0.39	1.07

Table 1. Calculated adsorption energy, intermolecular distance and maximum charge transfer at ground state.

The adsorption energy was calculated using Equation-1, the intermolecular distance is defined as the minimum distance between the anchoring atom of respective functional groups to the nearest titanium atom on the TiN(200) surface. The intermolecular charge transfer was computed in the similar way to Equation-1, except that the energy terms were replaced by the Löwdin charges (Löwdin 1950) as shown in the equation below,

$$C_{transfer} = C_{TiN(200)+Biotin(fg)} - C_{TiN(200)} - C_{Biotin(fg)}. \quad (3)$$

As indicated in Table 1, the most preferred orientation is the flat geometry shown in Fig. 1c, due to the most negative adsorption energy being calculated at the ground state. For the flat geometry, the intermolecular distance between the two nearest atoms of biotin and the TiN(200) surface is 2.27 Angstrom, i.e. the second closest among other configurations. With the electron population analysis of Equation-3, the maximum intermolecular charge transfer from biotin to the TiN(200) with the flat geometry is about 1.0 electron. The distribution of the electron transfer is further elucidated by the graphical representation in Fig. S8. With blue indicating accumulation and red showing removal of electrons, it can be observed from Fig. S7c that electrons are transfer from multiple atoms of biotin to the TiN(200) surface via the flat geometry. This is further illustrated by the top view in Fig. S8c. In comparison with other configurations, the carbonyl and carboxyl groups show significant charge transfer via the oxygen atom towards the TiN(200) surface as shown in Fig. S7a and Fig. S7b. Dominant charge transfers from the oxygen atoms of the flat configuration to the surface are also observed in Fig. S7c and Fig. S8c. However, the amine functional group only shows marginal charge transfer in Fig. S7d and Fig. S8d, which implies the absence of chemical bond formation. For the sulfide group, the dominant charge transfer is observed on the oxygen atom further away from the surface, whereas the valence electrons of the sulfur atom shows much less influence by the surface. Therefore, it may imply that titanium-sulfur interaction is rather weak in comparison to titanium-oxygen reaction. Therefore, the adsorption of biotin on TiN(200) surface may be classified into two different categories, 1) strong chemisorption by formation of chemical bonds via the carbonyl or carboxyl groups or both via the flat stacking orientation; 2) weak physisorption probably via van de Waals force by the amine and the sulfide groups.

To further verify the above statements, projected density of states (PDOS) of selected bonding atoms of each configuration were obtained and are shown in Fig. S9. The PDOS aids to visualize the hybridization of valence electronic orbitals, thus providing evidences on bond formation. Referring to the arrows of Fig. S9c, hybridization can be observed on the Ti $3d^2$, O $2p^4$, C $2p^2$, and N $2p^3$ orbitals at (i) -3.8 eV, (ii) -4.6 eV and (iii) -8.8 eV. Such hybridizations indicate formation of chemical bonds and these are in good agreement with the observation made by intermolecular charge transfer. For the case of carbonyl group in S8a, the general trend of hybridization is good. However, hybridization of Ti $3d^2$, O $2p^4$ and N $2p^3$ is surprisingly low at -4.6 eV. Therefore, the chemical bond may be relatively weak and the adsorption energy is reduced. Similar observation can be made in Fig. S9b, the carboxyl group at -4.6 eV where the Ti $3d^2$ shows little hybridization with O $2p^4$ and C $2p^2$. For the amine group in Fig. S9d, the Fermi level is shifted by about 0.2 eV towards negative, so the Ti $3d^2$ peak at -4.6 eV is shifted to -4.8 eV. However, the O $2p^4$ and N $2p^3$ are shifted by 0.2 eV towards positive. Therefore, hybridization is reduced. Finally, the sulfide group in Fig. S9e show even less hybridization as the Fermi level is shifted by 0.5 eV towards negative. There is little hybridization of the Ti $3d^2$ and S $3p^4$ orbitals, therefore chemical bond formation is impossible. With the charge analysis and PDOS data, we are convinced that chemisorption of biotin on TiN(200) is feasible via the titanium-oxygen reaction of carbonyl and carboxyl functional groups. The most stable adsorption geometry is likely to be the flat stacking configuration. The amine and sulfur functional groups may offer physisorption but these are less stable as predicted by DFT computation.

4. Conclusions

In this report, TiN thin films have been successfully synthesized with RF reactive sputtering technique and investigated as an alternative SPR sensing medium for ambient environment detection and biosensing in visible region. By optimizing the film thickness, the synthesized TiN film with thickness of 29.8 nm exhibits strong SPR absorption in the middle of visible region, competitive sensitivity of 1.93×10^{-7} RIU with differential phase modulation, and wide dynamic range of 3.2×10^{-2} RIU toward the ambient RI change. Furthermore, synthetic TiN films show unique bioaffinity toward biotin molecule. The experimental and computational results indicated that TiN films have better adsorption to biotin molecules via the titanium-oxygen reaction and formation of chemical bonds. The biotin-functionalized TiN film still shows good plasmonic sensing performance and good activity for further detection of streptavidin. These experimental and numerical proofs have successfully indicated, for the first time, that the TiN film can be functionalized with biotin molecules. By employing the biotinylation method, TiN thin film should be feasible for a wide range of plasmonic biosensing applications including the detection of proteins and DNA. In consideration of its excellent mechanical properties over conventional gold materials, TiN thin film can attract great interest in scientific and commercial biosensing applications.

References

Backmann, N., Zahnd, C., Huber, F., Bietsch, A., Pluckthun, A., Lang, H.P., Guntherodt, H.J., Hegner, M., Gerber, C., 2005. Proceedings of the National Academy of Sciences of the United States of America 102, 14587-14592.

Balamurugan, S., Obubuafo, A., Soper, S.A., Spivak, D.A., 2008. Analytical and Bioanalytical Chemistry 390, 1009-1021.

Chen, H.C., Tseng, B.H., Houng, M.P., Wang, Y.H., 2003. Thin Solid Films 445, 112-117.

Chin, Y.L., Chou, J.C., Lei, Z.C., Sun, T.P., Chung, W.Y., Hsiung, S.K., 2001. Japanese Journal of Applied Physics Part 1-Regular Papers Short Notes & Review Papers 40, 6311-6315.

Chun, S.Y., 2013. Journal of Nanoscience and Nanotechnology 13, 2021-2024.

Comin, A., Manna, L., 2014. Chemical Society Reviews 43, 3957-3975.

Cortie, M.B., Giddings, J., Dowd, A., 2010. Nanotechnology 21.

Dong, S.M., Chen, X., Gu, L., Zhang, L.X., Zhou, X.H., Liu, Z.H., Han, P.X., Xu, H.X., Yao, J.H., Zhang, X.Y., Li, L.F., Shang, C.Q., Cui, G.L., 2011. Biosensors & Bioelectronics 26, 4088-4094.

Elstner, F., Ehrlich, A., Giegengack, H., Kupfer, H., Richter, F., 1994. Journal of Vacuum Science & Technology a-Vacuum Surfaces and Films 12, 476-483.

Fredriksson, S., Gullberg, M., Jarvius, J., Olsson, C., Pietras, K., Gustafsdottir, S.M., Ostman, A., Landegren, U., 2002. Nature Biotechnology 20, 473-477.

Giannozzi, P., Baroni, S., Bonini, N., Calandra M., Car, R., Cavazzoni, C., Ceresoli, D., Chiarotti, G. L., Cococcioni, M., Dabo I., Dal Corso, A., Fabris, S., Fratesi, G., de Gironcoli, S., Gebauer, R., Gerstmann, U., Gougoussis, C., Kokalj, A., Lazzeri, M., Martin-Samos, L., Marzari, N., Mauri, F., Mazzarello, R., Paolini, S., Pasquarello, A., Paulatto, L., Sbraccia, C., Scandolo, S., Sclauzero, G., Seitsonen, A. P., Smogunov, A., Umari, P., Wentzcovitch, R. M., 2009. J. Phys. Condens. Matter 21, 395502.

Grimme, S., 2006. Journal of Computational Chemistry 27, 1787-1799.

Guler, U., Shalaev, V.M., Boltasseva, A., 2015. Materials Today 18, 227-237.

Haldorai, Y., Hwang, S.K., Gopalan, A.I., Huh, Y.S., Han, Y.K., Voit, W., Sai-Anand, G., Lee, K.P., 2016. Biosensors & Bioelectronics 79, 543-552.

He, J.L., Kou, W., Li, C., Cai, J.J., Kong, F.Y., Wang, W., 2015. International Journal of Electrochemical Science 10, 10074-10082.

Hlubina, P., Lunacek, J., Ciprian, D., Chlebus, R., 2008. Optics Communications 281, 2349-2354.

Homola, J., Yee, S.S., Gauglitz, G., 1999. Sensors and Actuators B-Chemical 54, 3-15.

Ishii, S., Sugavaneshwar, R.P., Nagao, T., 2016. Journal of Physical Chemistry C 120, 2343-2348.

Kanehara, M., Koike, H., Yoshinaga, T., Teranishi, T., 2009. Journal of the American Chemical Society 131, 17736-17737.

Kabashin, A. V., P. Evans, S. Pastkovsky, W. Hendren, G. A. Wurtz, R. Atkinson, R. Pollard, V. A. Podolskiy, and A. V. Zayats. 2009. Nature materials, 8, 867-871.

Kong, F.Y., Chen, T.T., Wang, J.Y., Fang, H.L., Fan, D.H., Wang, W., 2016. Sensors and Actuators B-Chemical 225, 298-304.

Lejaeghere, K., Bihlmayer, G., Björkman, T., Blaha, P., Blügel, S., Blum, V., Caliste, D., Castelli, I. E., Clark, S. J., and Dal Corso, A., 2016. *Science* 351, aad3000

Li, J.G., Gao, L., Sun, J., Zhang, Q.H., Guo, J.K., Yan, D.S., 2001. Journal of the American Ceramic Society 84, 3045-3047.

Liedberg, B., Nylander, C., Lundstrom, I., 1983. Sensors and Actuators 4, 299-304.

Liu, M.Y., Ma, Y.L., Su, L., Chou, K.C., Hou, X.M., 2016. Analyst 141, 1693-1699.

Löwdin, P.-O., 1950. Journal of Chemical Physics 18, 365.

Major, B., Mroz, W., Wierchon, T., Waldhauser, W., Lackner, J., Ebner, R., 2004. Surface & Coatings Technology 180, 580-584.

Mann, D.M., Broida, H.P., 1973. Journal of Applied Physics 44, 4950-4955.

Mayer, K.M., Hafner, J.H., 2011. Chemical Reviews 111, 3828-3857.

Michelotti, F., Dominici, L., Descrovi, E., Danz, N., Menchini, F., 2009. Optics Letters 34, 839-841.

Monkhorst, H. J., and Pack, J. D., 1976. Physical Review B 13, 5188

Naldoni, A., Guler, U., Wang, Z., Marelli, M., Malara, F., Meng, X., Besteiro, L.V., Govorov, A.O., Kildishev, A.V., Boltasseva, A. and Shalaev, V.M., 2017. Advanced Optical Materials. Doi: 10.1002/adom.201601031

Naik, G.V., Schroeder, J.L., Ni, X.J., Kildishev, A.V., Sands, T.D., Boltasseva, A., 2012. Optical Materials Express 2, 478-489.

Ng, S.P., Loo, F.C., Wu, S.Y., Kong, S.K., Wu, C.M.L., Ho, H.P., 2013. Optics Express 21, 20268-20273.

Ng, S.P., Wu, C.M.L., Wu, S.Y., Ho, H.P., 2011. Optics Express 19, 4521-4527.

PalDey, S., Deevi, S.C., 2003. Materials Science and Engineering a-Structural Materials Properties Microstructure and Processing 342, 58-79.

Patsalas, P., Charitidis, C., Logothetidis, S., 2000. Surface & Coatings Technology 125, 335-340.

Patsalas, P., Kalfagiannis, N., Kassavetis, S., 2015. Materials 8, 3128-3154.

Perdew, J.P., Burke, K., Ernzerhof, M., 1996. Physical Review Letters 77, 3865-3868.

Qiu, G.Y., Ng, S.P., Wu, C.M.L., 2015. Optics Letters 40, 1924-1927.

Schuller, J.A., Barnard, E.S., Cai, W.S., Jun, Y.C., White, J.S., Brongersma, M.L., 2010. Nature Materials 9, 193-204.

Shankaran, D.R., Gobi, K.V.A., Miura, N., 2007. Sensors and Actuators B-Chemical 121, 158-177.

Tian, Y., Tatsuma, T., 2005. Journal of the American Chemical Society 127, 7632-7637.

Uechi, I., Yamada, S., 2008. Analytical and Bioanalytical Chemistry 391, 2411-2421.

Venugopal, N., Gerasimov, V.S., Ershov, A.E., Karpov, S.V., Polyutov, S.P., 2017. Optical Materials 72, 397-402.

Vo-Dinh, T., Cullum, B., 2000. Fresenius Journal of Analytical Chemistry 366, 540-551.

Wang, J.G., Zhang, W.L., Zhu, M.P., Yi, K., Shao, J.D., 2015. Plasmonics 10, 1473-1478.

Weast, R.C., 1988. CRC handbook of chemistry and physics, 1st Student ed. CRC Press, Boca Raton, FL.

Weimer, W.A., Dyer, M.J., 2001. Applied Physics Letters 79, 3164-3166.

Zhao, J.H., Lin, J., Wei, H.Y., Li, X.H., Zhang, W.J., Zhao, G.N., Bu, J.L., Chen, Y., 2015. Optical Materials 47, 219-224.

Highlights:

- Titanium nitride (TiN) thin film for alternative surface plasmon resonance biosensors;
- Phase modulated highly sensitive TiN sensor for bulk refractive index sensing;
- Direct adsorption of biotin molecules on TiN thin film for potential label free biosensing;
- Computational study of biotin adsorption mechanism onto TiN(200) surface.